Dedicated Random Telegraph Noise Characterization of Ni/HfO$_2$-based RRAM Devices

M.B. Gonzalez[a*], J. Martin-Martinez[b], R. Rodriguez[b], M.C. Acero[a], M. Nafria[b],
F. Campabadal[a], X. Aymerich[b]

[a]*Institut de Microelectronica de Barcelona, IMB-CNM (CSIC), Campus UAB, 08193 Bellaterra, Spain*
[b]*Universitat Autonoma de Barcelona. Dept. Enginyeria Electronica Edifici Q. 08193 Bellaterra, Spain*
[*] Corresponding author: mireia.bargallo.gonzalez@csic.es

Abstract

In this work, random telegraph noise (RTN) associated to discrete current fluctuations in the high resistive state of Ni/HfO$_2$-based RRAM Devices is investigated. For this purpose, a dedicated software tool has been developed to control the instrumentation and to perform successive and smart RTN measurements in the time domain. After data acquisition, the advanced Weighted Time Lag (WTL) method is employed to accurately identify the contribution of multiple electrically active defects in multilevel RTN signals. Finally, the internal dynamics of trapping and de-trapping processes through the defects close to the filamentary path and its dependence on voltage and time are analyzed.

Keywords: Conductive filament, HfO$_2$, Ni, resistive random access memory (RRAM), random telegraph noise (RTN), variability.

1. Introduction

Filamentary resistive random access memory (RRAM) devices are considered the most promising candidate for next generation non-volatile memories due to their high scalability, fast switching speed, low power consumption, and high density 3-D integration [1]. However, before the commercial exploitation of this emerging technology, two major concerns need to be solved: device endurance and switching variability. In order to determine the reliability and stochastic variability of the memory performance, a better understanding of random telegraph noise (RTN) in RRAM cells is required, as it can cause severe operation or read errors [2-14].

Besides that, RTN reveals the internal dynamics of electrically active defects, being related to the physical nature of the material, interface, and conductive filament (CF) properties. Hence an in depth analysis of the RTN spectra will also provide a deeper insight in the device physics, and allow testing hypotheses about the nature of grown-in defects and the key transport mechanisms involved in the switching phenomenon. In this work, dedicated characterization techniques are employed to obtain a better understanding of the discrete current fluctuations in the high resistive state (HRS), due to electron capture and emission processes through defects close to the filamentary path [4,8-9,14].

2. Experimental

2.1. Device Description

The Ni/HfO$_2$/Si devices were fabricated on (100) n-type CZ silicon wafers with resistivity (7-13) mΩ·cm following a field isolated process. The 20nm-thick HfO$_2$ layers were deposited by ALD at 498K using TDMAH and H$_2$O as precursors. The resulting structures are square cells of 5x5μm^2. A schematic cross-section of the final device is shown in Fig. 1(a). More detailed information about the process flow can be found in Ref. [15].
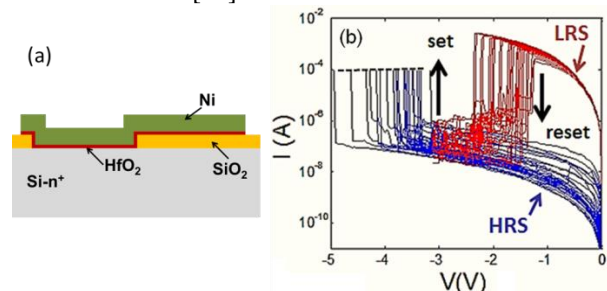

Fig. 1. (a) Schematic cross-section of the studied devices. (b) Unipolar resistive-switching behavior of Ni/HfO$_2$-based devices during set and reset operations.

2.2. Characterization Setup

The current-time traces were recorded in the HRS, which shows higher RTN fluctuations than the low resistive state (LRS) [4, 8-9]. The measurements have been done at 300K using an HP-4155B semiconductor

parameter analyzer. The voltage was applied to the top Ni electrode, while the Si substrate was grounded.

In order to optimize the detection of the occasionally appearing RTN signal, smart decisions are needed to be automatically taken considering the previously recorded result. These decisions could request to measure at a new voltage, or to force a new switching cycle when the measured current values are not optimal for RTN detection. For this purpose, a software tool to control the instrumentation and to perform numerous and smart measurements has been designed and developed in Matlab®. A flow chart of the algorithm employed for the RTN measurements is shown in Fig. 2.
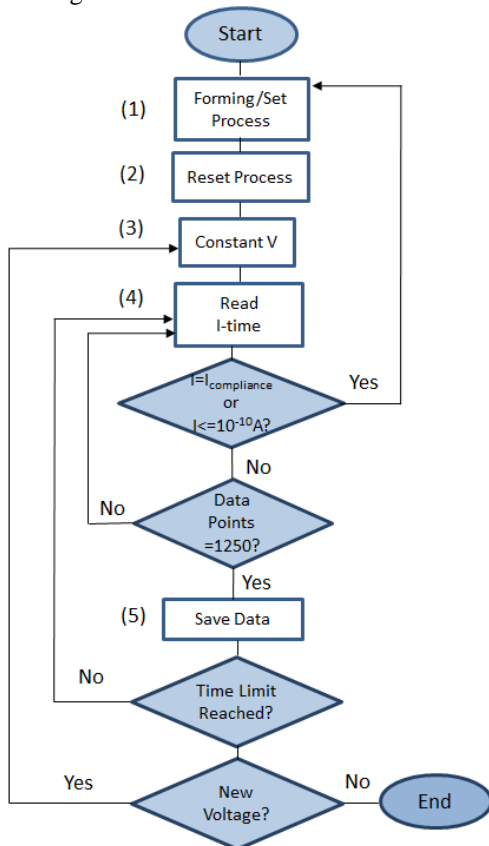

Fig. 2. Flow chart of the algorithm employed for the RTN measurements.

Furthermore, the recently published advanced Weighted Time Lag (WTL) method [16,17] was employed to accurately identify the discrete current levels and to minimize the negative effect of the background noise.

3. Results and Discussion

Fig. 1(b) shows typical unipolar switching behavior for the studied Ni/HfO$_2$-based resistive switching structures [15] after an initial forming

operation at a voltage ~ -11V. When a constant voltage is applied in the HRS, RTN fluctuations due to electron trapping and de-trapping processes can be detected. In Fig. 3, typical RTN signals in the HRS of the studied devices are shown. Note that the observed RTN spectra can be attributed to standard and anomalous defect configurations, which are commonly observed in deep sub-micron MOSFETs [18,19]. The evidenced charge transitions from the different states involve an excitation over an energy barrier (Fig. 4) with a field and temperature dependent emission and capture time constants. In the case of the anomalous RTN (Fig. 4 right), one additional metastable state is introduced. In this state, the defect remains in a negatively charged state and the RTN pauses [18,19]. As a result, the current will remain in the low level. RTN fluctuations will be again observed once a charge transition with longer switching rates (owing to a higher energy barrier) arises.
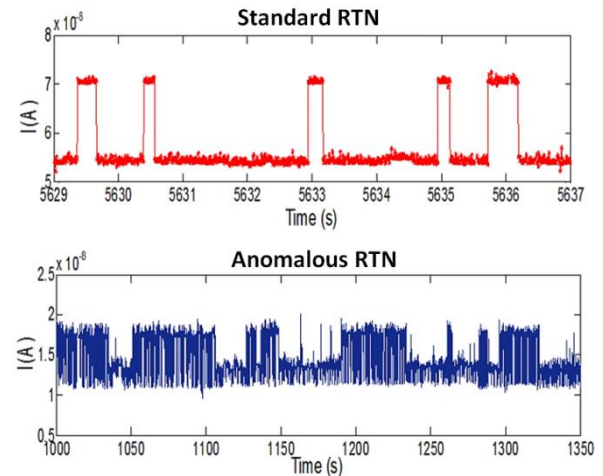

Fig. 3. RTN fluctuations in the high resistive state, owing to standard (top) and anomalous (bottom) defect configurations.
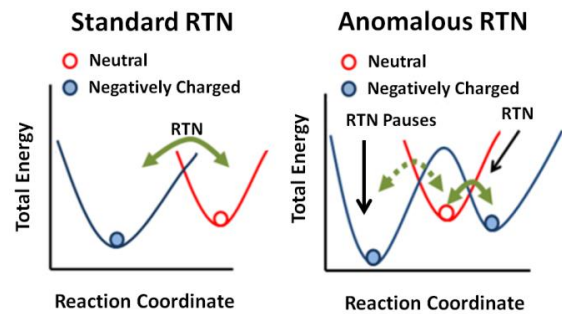

Fig. 4. Possible configuration coordinate diagrams of RTN fluctuations corresponding to Fig. 3, owing to a standard (left) and anomalous (right) defect configurations.

Notice, that the contribution of RTN instabilities in the HRS is significantly smaller than the memory window in the studied devices (see Fig.1). Therefore,
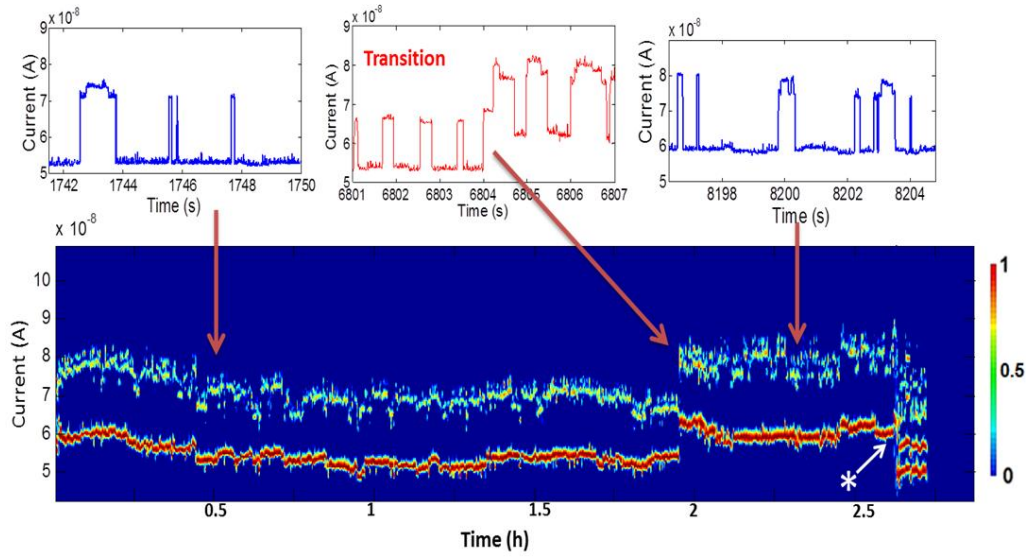
Fig. 5. Typical RTN fluctuations of the current in the HRS measured at -0.5V (top). Evolution of the detected current levels and their probabilities of occurrence over the measuring time. The values have been calculated by applying the WTL method [16] to the experimental signal.

the detected current fluctuations would not cause an erroneous read of the memory state. However, further work should be done to investigate the joint impact of irreversible digital-like current changes, (owing to trap density variations inside or near the conductive filament [4]), and RTN fluctuations on the memory performance.
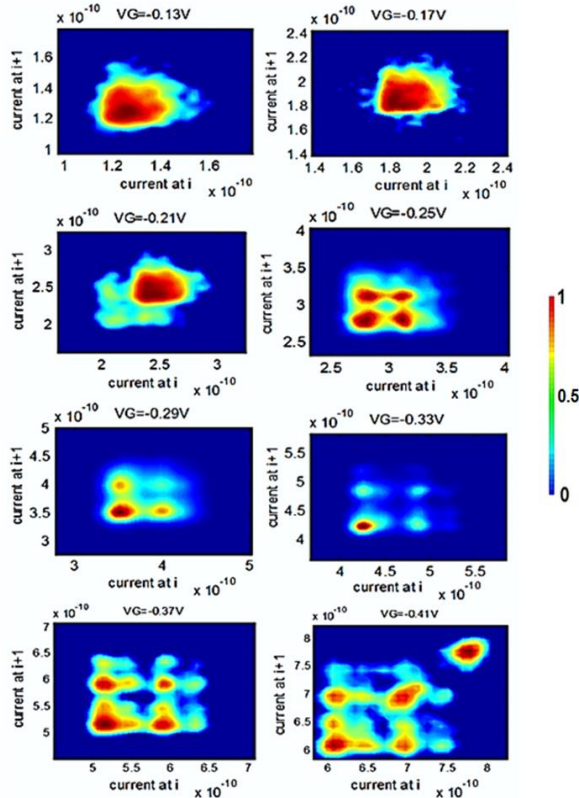

Fig. 6. WTL plots of the current (in A) in the HRS at several voltages, where 1250 data points were acquired at each voltage condition.

To obtain a better understanding of the RTN phenomenon in long measurements, a constant voltage (-0.5V) was applied during ~3 hours with a time resolution of 8.7ms, leading to ~1.2×10^6 data points. Fig. 5 (bottom) shows the probability that a single point with coordinates (current at i, current at i+1) of the WTLP space (see Fig. 6) corresponds to a current level. These values have been evaluated from the maximums of the diagonals of WTLPs, since each of these maximums corresponds to a current level of the RTN signal [16]. This method allows to accurately identify the current levels by minimizing the negative effect of the background noise. The plots in the top of Fig. 5 correspond to selected time intervals of the RTN measurement. Notice that a standard RTN signal is clearly observed during the first two hours (Fig. 5 top-left). Next, a clear current jump from 6.6×10^{-8}A to 8×10^{-8}A is detected (Fig. 5 top-middle). This current increase can be attributed to a charge capture or emission processes from a trap state with longer emission/capture time constants than those previously detected [18]. After that, a standard RTN signal with larger current values is observed (Fig. 5 top-right). Finally, after 2.6h (marked with *), a charge transition from the same trap takes place. This fact indicates that for a proper evaluation of the RTN impact in RRAM performance prolonged times should be assessed.

In order to analyze the impact of the voltage on the current fluctuations, 50 different voltages were evaluated. The measurement started at -0.1V, and every 1250 data points the voltage was varied from -0.1V to -0.6V.

Fig. 6 shows several WTL plots obtained by applying the WTL method [16] to the RTN traces

measured at different voltage conditions. It should be mentioned that the color bar indicates the probability to find a current value at certain moment (current at i+1) versus the previous value (current at i). In these plots the peaks at the diagonal x-axis=y-axis indicate the RTN levels, while peaks outside the diagonal correspond to transitions between these current levels.
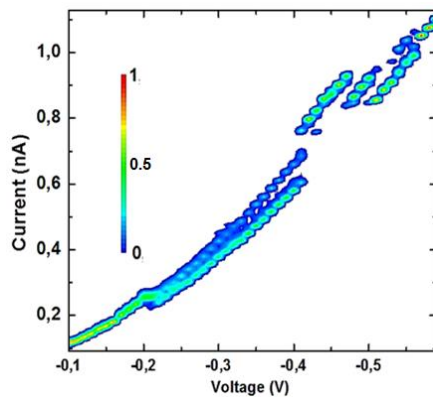

Fig. 7. RTN current levels versus applied voltage, where the color code indicates the probability to find a current level. The observed values have been obtained from the diagonal of 50 WTL plots, corresponding to 50 different voltages.

From the plots of Fig. 6, it can be observed that until -0.2V only one level in the diagonal can be distinguished. However, in the voltage range from -0.21V to -0.41V at least two peaks are clearly visible across the diagonal. These peaks indicate that more than one current level is detected as a result of the RTN activation. Fig. 7 shows the observed current levels versus voltage for all the voltage range assessed. Notice that each voltage assessed has a different WTLP (see Fig. 6), and that the number of levels and their probabilities of occurrence significantly depend on the applied voltage. This result evidences the activation/deactivation of charge transitions between energetic states, when their associated energy barriers (Fig. 4) are modified with voltage.

4. Conclusions

The presence of electrically active defects responsible for the RTN signal in Ni/HfO_2-based RRAM devices has been investigated using an advanced RTN characterization technique. The results show that the electron capture and emission processes through defects in the vicinity of the conductive filament have a marked impact on the electrical response. Moreover, the internal dynamics of defects responsible for the current fluctuations and its time and voltage dependence are analyzed.

References

[1] R. Waser, M. Aono, Nature Mater. 6 (2007) 833.
[2] R. Soni, P. Meuffels, A. Petraru, M. Weides, C. Kügeler, R. Waser, H. Kohlstedt, J. Appl. Phys. 107 (2010) 024517.
[3] Y. H. Tseng, W. C. Shen, C. J. Lin, J. Appl. Phys. 111 (2012) 073701.
[4] D. Veksler, G. Bersuker, B. Chakrabarti, E. Vogel, S. Deora, K. Matthews, D. C. Gilmer, H.-F. Li, S. Gausephol, P. D. Kirsch, in Proc. IEDM (2012) 9.6.1.
[5] F.M. Puglisi, P. Pavan, A. Padovani, L. Larcher, G. Bersuker, Solid-State Electron. 84 (2013) 160.
[6] N. Raghavan, R. Degraeve, A. Fantini, L. Goux, S. Strangio, B. Govoreanu, D. J. Wouters, G. Groseneken, M. Jurczak, in Proc. IRPS (2013) 5E.3.1.
[7] Y. J. Huang, S. S. Chung, H. Y. Lee, Y. S. Chen, F. T. Chen, P. Y. Gu, M.-J. Tsai, in Proc. IRPS (2013) MY.3.1.
[8] D. Veksler, G. Bersuker, L. Vandelli, A. Padovani, L. Larcher, A. Muraviev, B. Chakrabarti, E. Vogel, D. C. Gilmer, P. D. Kirsch, in Proc. IRPS (2013) MY.10.1.
[9] Y. Zhang, H. Wu, M. Wu, N. Deng, Z. Yu, J. Zhang, H. Qian, Appl. Phys. Lett. 104 (2014) 103507.
[10] S. Choi, Y. Yang, W. Lu, Nanoscale 6 (2014) 400.
[11] Y. T. Chung, Y. H. Liu, P. C. Su, Y. H. Cheng, T. Wang, M. C. Chen, in Proc. IRPS (2014) MY.2.1.
[12] S. Ambrogio, S. Balatti, A. Cubeta, A. Calderoni, N. Ramaswamy, D. Ielmini, IEEE Trans. Electron Devices 61 (2014) 2912.
[13] S. Balatti, S. Ambrogio, A. Cubeta, N. Ramaswamy, D. Ielmini, in Proc. IRPS (2014) MY4.1.
[14] F. M. Puglisi, L. Larcher, P. Pavan, A. Padovani, G. Bersuker, in Proc. IRPS (2014) MY.5.1.
[15] M. B. Gonzalez, J. M. Rafí, O. Beldarrain, M. Zabala, M. C. Acero, F. Campabadal, IEEE Trans. Device Mater. Reliab. 14 (2014) 769.
[16] J. Martin-Martinez, J. Diaz, R. Rodriguez, M. Nafria, X. Aymerich, IEEE Electron Device Lett. 35 (2014) 479.
[17] M. Maestro, J. Diaz, A. Crespo-Yepes, M.B. Gonzalez, J. Martin-Martinez, R. Rodriguez, F. Campabadal, M. Nafria, X. Aymerich Proc. EUROSOI-ULIS 2015, 133-136.
[18] T. Grasser, Microelectron. Reliab 52 (2012) 39.
[19] M. J. Uren, M. J. Kirton, S. Colins, Phys. Rev. B 37 (1988) 8346.